Two-dimensional waves in a chiral elastic chain: dynamic Green's matrices and localised defect modes

I.S. Jones[1], **N.V. Movchan**[2], **A.B. Movchan**[2]

[1] Liverpool John Moores University, Mechanical Engineering and Materials Research Centre, Liverpool, L3 3AF, UK

[2] University of Liverpool, Department of Mathematical Sciences, Liverpool, L69 7ZL, UK

Abstract

This paper presents new analytical work on the analysis of waves in chiral elastic chains. The notion of dynamic chirality, well established and explored for electromagnetic waves in magnetised media, is less common for elastic solids. Indeed, it is even less common to observe vector wave problems in an elastic chain. Here, it is shown that the physical system, described by a vector formulation for waves in a chiral chain, can simultaneously support Floquet-Bloch waves in addition to localised waveforms, subject to the appropriate choice of the frequency interval. We construct and analyse dynamic Green's matrices and identify exponentially localised defect modes, which correspond to spatially confined elliptical motion of nodal inertial elements, around the perturbed cell of the chiral chain. Special attention is given to the case of the dynamic degeneracy. Analytical findings are accompanied by numerical illustrations and examples.

1 Introduction

A model is presented here which incorporates a constructive mechanism of chiral coupling for a lattice wave system. The analysis and simulations are carried out in the context of mathematical elasticity and hence appropriate terminology is used such as the stiffness matrix, displacements and forces. The results of the analysis may be applied in a wider context. For specific considerations, formal derivations are given for an elastic chiral chain, characterised by a symmetric, real-valued stiffness matrix and a Hermitian matrix of inertia.

Effects of chirality in electro-magnetic waves in magnetised media are well represented in the literature (see for example, [**?**, **?**, **?**, **?**]) and often, for structured systems, are associated with non-reciprocity [**?**, **?**]. It is also known that Floquet-Bloch waves within periodic systems may possess unusual dispersion properties, which may include stop bands and dynamic anisotropy. These, in turn, may be connected to the transmission/reflection problems, negative refraction, as well as standing waves and localised defect modes [**?**, **?**, **?**, **?**].

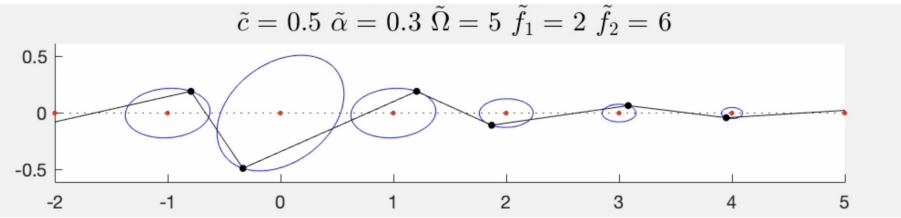

Figure 1: The resulting elliptical trajectories of nodes in an infinite chiral chain with pre-tension, when the central node ($n = 0$) is forced in a time-harmonic manner with force amplitude $(f_1, f_2) = (2, 6)$. The forcing frequency is chosen to be from the stop band. Parameter values: gyricity $\tilde{\alpha} = 0.3$, spectral parameter $\tilde{\Omega} = \omega^2 = 5$, pretension $\tilde{c} = 0.5$. Nodal trajectories for node labels $n = -1$ to $n = 4$ are shown.

Geometrically chiral elastic systems, both in statics and dynamics, have been discussed in [**?**, **?**, **?**, **?**], where the emphasis is on structural elements which couple rotational displacements and dilatational deformation.

Another class of chiral systems, based on periodically embedded gyroscopes of given translational and rotational inertia, was studied in [**?**, **?**, **?**, **?**, **?**]. Specifically, the lattice characteristics of polarisation and vortex waves were presented in [**?**]. In [**?**], it has been shown that vortex waves represent a new class of waveforms, not observed in conventional non-chiral media.

In the present paper, the problem is formulated for an infinite chain of inertial elements, which possess translational and gyroscopic rotational inertia; an allowance is also made for a pre-tension along the chain. Even though the chain is geometrically one-dimensional, elastic waves induce both longitudinal and transverse displacements. For a chain of point masses, connected by massless elastic links, longitudinal and transverse displacements are entirely decoupled. However, the inertia of the gyroscopic chiral elements yields a Hermitian matrix inertia term in the governing equations. Consequently, this brings a coupling between the transverse and longitudinal displacements, and in a selected time-harmonic regime, two-dimensional orbits are observed along the vibrating chain.

Dispersion of vector Floquet-Bloch waves in a chiral elastic chain is particularly interesting due to the presence of stop bands and partial pass bands, in addition to degeneracies associated with the elastic stiffness. The unusual structure of the waveforms, associated with the chirality-induced asymmetry, is also noted.

Dynamic Green's matrices and, in particular, stop-band Green's matrices are of special interest. Here, closed form analytical representations of the fundamental solutions are derived and several illustrations of the forced vibrations are given. In particular, exponentially localised vibrations (with the forcing frequency chosen from the stop-band range) are shown in Fig. **??** for the chiral elastic chain due to the action of an oblique force applied to the node labelled $n = 0$. A special feature is the presence of elliptical trajectories of the nodal elements. Detailed discussion of the simulation is included in Section **??**.

Dynamic degeneracy occurs when the transverse pre-tension becomes zero. In this case, the nature of the chiral coupling and the dynamic response of the chiral elastic chain deserve special attention which is afforded in the present text. We show that the motion of the nodal inertial elements occurs in elliptical orbits which may be aligned in a longitudinal or transverse direction, even though the force at the origin may be applied at an oblique angle to the chain. Dynamic Green's matrices are derived in a closed analytical form, and their properties reveal the special features of the chiral elastic system with dynamic degeneracy.

Exponentially localised chiral defect modes are shown to exist in a chiral chain, characterised by a perturbation of both translational and rotational inertia at the central cell, located at the origin ($n = 0$), with no additional external forcing present. Such non-trivial solutions have been constructed and analysed here.

The structure of the paper is as follows. Floquet-Bloch waves in a chiral elastic system are analysed in Section **??**. Green's matrices for pass band, partial pass band and stop band regimes are derived and discussed in Section **??**, together with "one-sided" Green's matrices. An asymmetrically localised Green's matrix is constructed in Section **??**. Section **??** presents the special case of the dynamic degeneracy for the chiral elastic system. Exponentially localised chiral defect modes are considered in Section **??**, followed by the concluding discussion.

2 Floquet-Bloch waves in a chiral chain with existing pre-tension

2.1 Governing equations

In a chiral chain, characterised by a chirality parameter α, consider a vector time-harmonic wave of complex amplitude $\mathbf{U}^{(n)} = (U_1^{(n)}, U_2^{(n)})^T$, such that

$$-m\omega^2\mathbf{U}^{(n)} = \mathbf{C}(\mathbf{U}^{(n-1)} + \mathbf{U}^{(n+1)} - 2\mathbf{U}^{(n)}) + i\alpha\omega^2\mathbf{R}\mathbf{U}^{(n)}. \tag{1}$$

The system of equations (**??**) may be linked to an electromagnetic wave in a periodically magnetised medium, or to a mechanical wave in an elastic, pre-tensed, infinite string with periodically distributed masses attached to gyroscopic spinners.

In the context of elasticity, m is the common mass of the nodal points labelled by the integer n, ω is the radian frequency of the wave, and $\mathbf{C}, \mathbf{R}$ are the stiffness and rotation matrices respectively,

$$\mathbf{C} = \begin{pmatrix} c_1 & 0 \\ 0 & c_2 \end{pmatrix}, \quad \mathbf{R} = \begin{pmatrix} 0 & 1 \\ -1 & 0 \end{pmatrix}. \tag{2}$$

Here c_1 and c_2 represent the effective pre-tension in the connecting elastic elements. Assuming the spatial period is a, which represents the distance between the neighbouring nodal points, the quasi-periodic condition is imposed

$$\mathbf{U}^{(n+1)} = e^{ika}\mathbf{U}^{(n)}. \tag{3}$$

In the framework of the definition of the Floquet-Bloch waves, it is assumed that the phase shift between the displacements of neighbouring nodes is the same with respect to both directions (longitudinal and transverse components). The wave number is denoted by k. Hence, the system (**??**) is reduced to the form

$$\big[- m\omega^2\mathbf{I} - 2\big(\cos(ka) - 1\big)\mathbf{C} - i\alpha\omega^2\mathbf{R}\big]\mathbf{U}^{(n)} = \mathbf{0}. \tag{4}$$

Introduce the dimensionless variables:

$$\tilde{\mathbf{U}}^{(n)} = \frac{1}{a}\mathbf{U}^{(n)}, \quad \tilde{k} = ka, \quad \tilde{\alpha} = \frac{\alpha}{m}, \quad \tilde{\omega} = \omega\sqrt{\frac{m}{c_1}}, \quad \tilde{c} = \frac{c_2}{c_1}, \tag{5}$$

where the quantities with the symbol "$\sim$" are dimensionless. Equation (**??**) becomes (dropping the "$\sim$" for convenience)

$$\begin{aligned} -\omega^2 U_1^{(n)} &= 2(\cos k - 1)U_1^{(n)} + i\alpha\omega^2 U_2^{(n)}, \\ -\omega^2 U_2^{(n)} &= 2c(\cos k - 1)U_2^{(n)} - i\alpha\omega^2 U_1^{(n)}. \end{aligned} \tag{6}$$

2.2 Dispersion properties of the Floquet-Bloch waves

For non-trivial solutions of (**??**), it is required that

$$\sigma(\alpha, \omega, c, k) = 0, \tag{7}$$

where

$$\sigma(k, \alpha, \omega, c) = (1 - \alpha^2)\omega^4 - 2(c + 1)(1 - \cos k)\omega^2 + 4c(1 - \cos k)^2. \tag{8}$$

This gives the dispersion relation

$$(\omega^{\pm})^2 = \omega_0^2 P^{\pm}(\alpha, c), \tag{9}$$

where

$$P^{\pm}(\alpha, c) = \frac{(c + 1) \pm \sqrt{(c + 1)^2 - 4c(1 - \alpha^2)}}{2(1 - \alpha^2)}, \tag{10}$$

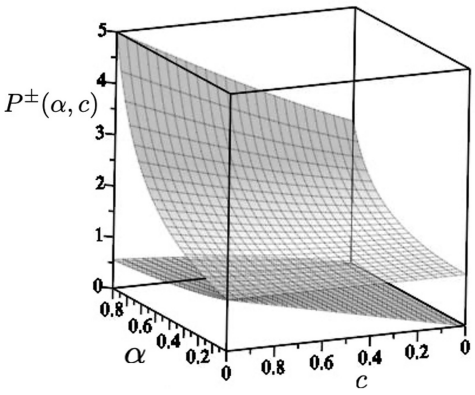

(a) The graphs of functions $P^{\pm}(\alpha, c)$, as defined in (**??**).

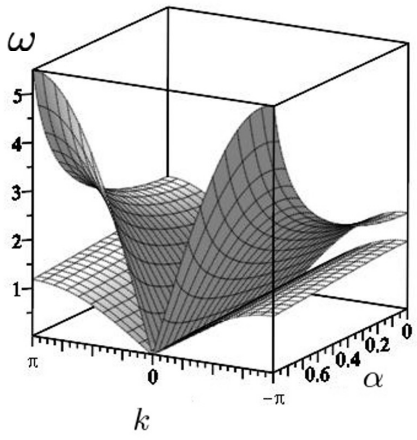

(b) The graphs of $\omega^{\pm}$ as functions of k and α, as defined in (**??**), for $c = 0.5$

Figure 2: Dispersion of Floquet-Bloch waves in a chiral periodic chain.

and ω_0 is the frequency of waves in the classical one-dimensional, monatomic, infinite chain, such that

$$\omega_0^2 = 2(1 - \cos k). \tag{11}$$

In the mechanical context, the separable nature of this result should be noted in that the frequency of the classical case of the one-dimensional monatomic chain is multiplied by the function $P^{\pm}(\alpha, c)$. The parameter c measures the degree of pre-tension in the string such that $0 \leq c < 1$ for a pre-tensioned chain. The parameter α indicates the effect of the gyroscopic spinners [**?**]. The dimensionless parameter c in (**??**) is given by $c = (a - l_0)/a$ where l_0 is the "natural length".

2.2.1 The role of pre-tension

For a chain with no transverse pre-tension ($c = 0$), there is a single mode with a non-zero frequency given by

$$\omega = \frac{\omega_0}{\sqrt{1 - \alpha^2}}. \tag{12}$$

The presence of pre-tension introduces an additional mode with non-zero frequency. For a chain with pre-tension but without spinners, the frequencies are given by

$$(\omega^+)^2 = \omega_0^2, \quad (\omega^-)^2 = c\omega_0^2. \tag{13}$$

There is clearly a degenerate point at $c = 1$ which corresponds to infinite pre-tension in the mechanical context.

The general behaviour of the frequencies of the modes for various values of α and c may be seen in Fig. **??** where the functions $P^{\pm}(\alpha, c)$ are plotted. The presence of an additional low frequency mode, which increases with increasing values of c, may be seen. The variation in ω as a function of both k and α is shown in Fig. **??** for $c = 0.5$. It is convenient to identify three regions along the frequency axis in Fig. **??**, which are typical of the dispersive behaviour for all $0 < c < 1$. For frequencies above both surfaces, there is a stop band. For frequencies below both surfaces there is a pass band, and for frequencies above the lower surface and below the upper surface, there will be a "partial pass band" with both evanescent and propagating modes present.

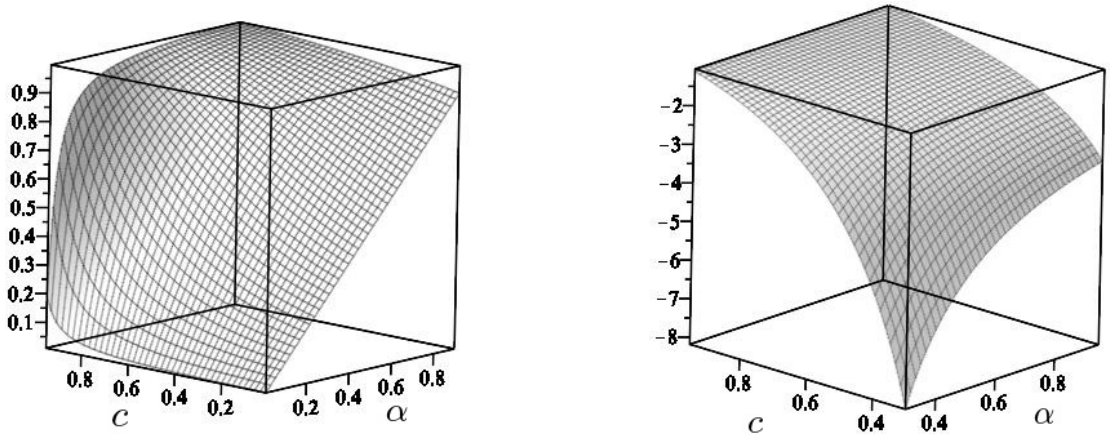

(a) The function $\frac{P^+(\alpha,c)-1}{\alpha P^+(\alpha,c)}$

(b) The function $\frac{P^-(\alpha,c)-1}{\alpha P^-(\alpha,c)}$

Figure 3: The coefficients of $x_1^{(n)}$ in (**??**) as functions of α and c.

2.2.2 The displacement amplitude

As follows from (**??**), (**??**), (**??**), the displacement amplitude eigenvectors, independent of k, are given by

$$\mathbf{U}_{\pm}^{(n)} = \Big(\frac{i\alpha P^{\pm}(\alpha,c)}{1-P^{\pm}(\alpha,c)}, 1\Big)^T. \tag{14}$$

The dimensionless time-harmonic displacements $\mathbf{u}_{\pm}^{(n)}$ of the eigenmodes are then given by

$$\mathbf{u}_{\pm}^{(n)} = \mathrm{Re}\Big(\mathbf{U}_{\pm}^{(n)} e^{i\omega t}\Big). \tag{15}$$

It is noted that the expression $(c+1)^2 - 4c(1-\alpha^2) \geq 0$ since $0 \leq \alpha < 1$ and $c \geq 0$. Hence $P^{\pm}(\alpha,c)$ are both real. Thus the first components of the eigenvectors in (**??**) are purely imaginary and hence the resulting elliptical trajectories have axes aligned parallel and perpendicular to the chain.

2.2.3 Elliptical trajectories of the nodal points

The equations of the trajectories of the nodal points are given by

$$\left(\frac{P^{\pm}(\alpha,c)-1}{\alpha P^{\pm}(\alpha,c)} x_1^{(n)}\right)^2 + x_2^{(n)2} = 1. \tag{16}$$

Here, $x_1^{(n)}$ and $x_2^{(n)}$ are the local coordinates associated with the elliptical trajectory at node n with local origin at the equilibrium position of node n; the $x_1^{(n)}$ axes are parallel to the chain in the direction of increasing n and the $x_2^{(n)}$ axes are perpendicular to the chain. The coefficients of $x_1^{(n)}$ for each mode are plotted in Fig. **??**. It may be seen that $|P^+(\alpha,c)| < 1$ and $|P^-(\alpha,c)| > 1$ throughout the (α,c) space. Thus the "+" mode is aligned with its major axis along the chain and the "-" mode is aligned with its major axis perpendicular to the chain in all cases.

Some typical modes are shown in Fig. **??** for various values of α and c. Increasing separately α or c decreases the eccentricity of the elliptical trajectory of the nodes.

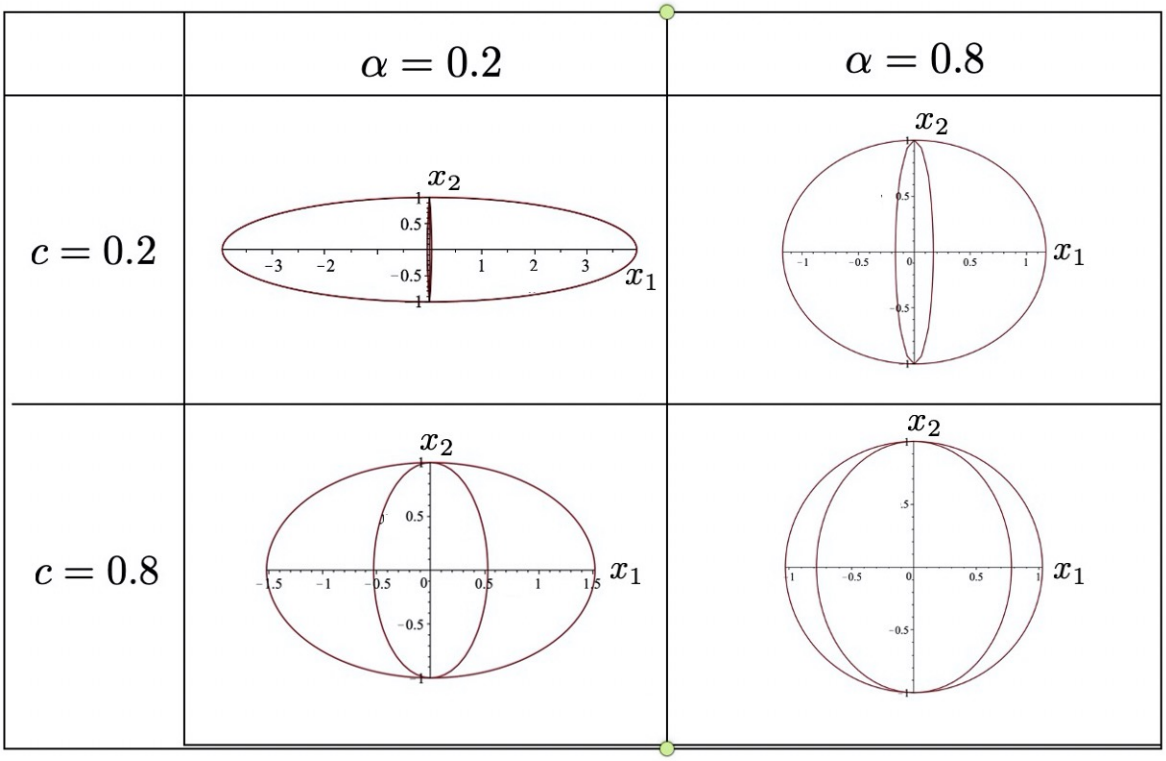

Figure 4: The mode shapes for an infinite chiral chain for a selection of values of α and c. The "+" mode is aligned with its major axis along the chain and the "-" mode is aligned with its major axis perpendicular to the chain in all cases.

Consider now a chain with pre-tension where there are two modes with non-zero frequency. Again from (**??**), the major axes of the two elliptical modes align parallel and perpendicular to the chain in view of the behaviour of the coefficients in (**??**). As $\alpha \to 0$, the ellipses in the two modes become more eccentric tending to linear motion parallel and perpendicular to the chain.

The asymptotic behaviour of the coefficients is summarised below.

(a) When c is fixed and $0 < c < 1$,

$$\frac{P^+(\alpha,c)-1}{\alpha P^+(\alpha,c)} \sim \frac{\alpha}{1-c} + O(\alpha^3) \quad \text{as} \quad \alpha \to 0, \tag{17}$$

$$\frac{P^-(\alpha,c)-1}{\alpha P^-(\alpha,c)} \sim \frac{c-1}{\alpha c} + O(\alpha) \quad \text{as} \quad \alpha \to 0. \tag{18}$$

(b) When α is fixed and $0 < \alpha < 1$,

$$\frac{P^+(\alpha,c)-1}{\alpha P^+(\alpha,c)} \sim \alpha + \alpha(1-\alpha^2)c + O(c^2) \quad \text{as} \quad c \to 0 \quad \text{for fixed } \alpha, \tag{19}$$

$$\frac{P^-(\alpha,c)-1}{\alpha P^-(\alpha,c)} \sim \frac{-1}{\alpha c} + O(c^0) \quad \text{as} \quad c \to 0 \quad \text{for fixed } \alpha. \tag{20}$$

The behaviour of the trajectories is completely described by equations (**??**), (**??**) and (**??**) with limiting behaviour described by (**??**) and (**??**)-(**??**).

For a chain with no transverse pre-tension ($c = 0$) (see (**??**)), there is only one mode (the "+" mode) with major axes of the nodal ellipses aligned parallel to the chain and the common equation of the nodal trajectory is given by

$$\Big(\alpha x_1\Big)^2 + x_2^2 = 1, \tag{21}$$

where x_1 and x_2 are generic local coordinates.

Additionally in this case, as $\alpha \to 0$, the ellipses become more eccentric tending to linear motion in the direction of the chain as $\alpha \to 0$. In the case of $c = 0$ (no transverse pre-tension), for maximum gyricity ($\alpha \to 1$), the trajectories tend towards circles.

3 Dynamic Green's kernel for a chiral chain

3.1 The infinite chiral chain with a time-harmonic force acting on the central node

Consider the chiral chain discussed above but with a time-harmonic force $(f_1, f_2)^T e^{i\omega t}$ acting at the central ($n = 0$) node. In the same dimensionless variables, the governing equations are

$$\begin{aligned} -\Omega U_1^{(n)} &= (U_1^{(n+1)} + U_1^{(n-1)} - 2U_1^{(n)}) + i\alpha\Omega U_2^{(n)} + \tilde{f}_1\delta_{n0}, \\ -\Omega U_2^{(n)} &= c(U_2^{(n+1)} + U_2^{(n-1)} - 2U_2^{(n)}) - i\alpha\Omega U_1^{(n)} + \tilde{f}_2\delta_{n0}, \end{aligned} \tag{22}$$

where $\Omega = \omega^2$ and $\tilde{f}_i = f_i/ac_1$.

By taking the discrete Fourier Transform of equations (**??**) with respect to a Fourier variable k, this leads to the solution

$$U_i^{(n)} = \sum_{j=1,2} G_{ij}^{(n)} f_j, \tag{23}$$

where the Green's matrix is given by

$$G_{ij}^{(n)} = \frac{1}{2\pi}\int_{-\pi}^{\pi} \hat{G}_{ij} e^{ikn}\, dk, \tag{24}$$

with

$$\hat{G}_{ij} = \frac{1}{\sigma(k,\alpha,\Omega,c)} \begin{pmatrix} 2c(1-\cos k) - \Omega & i\alpha\Omega \\ -i\alpha\Omega & 2(1-\cos k) - \Omega \end{pmatrix}. \tag{25}$$

Thus, the Green's matrix is given by

$$G^{(n)} = -\Omega F(n,\Omega,\alpha,c)(\mathbf{I} - \mathrm{i}\alpha\mathbf{R}) - \mathfrak{F}(n,\Omega,\alpha,c)\ \mathrm{diag}\{c,1\}, \tag{26}$$

where $\mathbf{I}$ is the 2×2 identity matrix and $\mathbf{R}$ is given in (**??**) with

$$F(n,\Omega,\alpha,c) = \frac{1}{2\pi}\int_{-\pi}^{\pi} \frac{e^{ikn}}{\sigma(k,\alpha,\Omega,c)}\, dk, \tag{27}$$

$$\begin{aligned} \mathfrak{F}(n,\Omega,\alpha,c) &= \frac{1}{\pi}\int_{-\pi}^{\pi} \frac{(\cos k - 1)e^{ikn}}{\sigma(k,\alpha,\Omega,c)}\, dk \\ &= F(n+1,\Omega,\alpha,c) - 2F(n,\Omega,\alpha,c) + F(n-1,\Omega,\alpha,c). \end{aligned} \tag{28}$$

3.2 Evaluation of $F(n, \Omega, \alpha, c)$

The evaluation of the integral in (**??**) will depend on whether the forcing frequency is in the stop band, pass band or partial pass band in the dispersion diagram. Hence the Green's matrix will take different analytical forms in these three regimes. The function $F(n, \Omega, \alpha, c)$ may be written as

$$F(n,\Omega,\alpha,c) = \frac{1}{2\pi\Omega(1-\alpha^2)(P^-(\alpha,c)-P^+(\alpha,c))}\int_0^\pi \frac{(\lambda^+-\lambda^-)\cos kn\ dk}{(\cos k-\lambda^-)(\cos k-\lambda^+)} \tag{29}$$

$$= \frac{1}{2\pi\Omega(1-\alpha^2)(P^-(\alpha,c)-P^+(\alpha,c))}\left[\int_0^\pi \frac{\cos kn\ dk}{(\cos k-\lambda^+)} - \int_0^\pi \frac{\cos kn\ dk}{(\cos k-\lambda^-)}\right],$$

where

$$\lambda^\pm = 1 - \frac{\Omega(1-\alpha^2)P^\pm(\alpha,c)}{2c}. \tag{30}$$

For convenience, introduce $a^\pm = \frac{1}{\lambda^\pm}$. The behaviour of $|a^\pm(\Omega,\alpha,c)|$ is crucial in the evaluation of the integral. Noting that $P^+P^- = c/(1-\alpha^2)$, and by examining the sign of $|a^\pm(\Omega,\alpha,c)|$, the value of the integral in (**??**), and hence the function $F(n,\Omega,\alpha,c)$, is determined. This leads to the following:

Pass band	$0 < \Omega < 4P^-$	$\lvert a^+\rvert > 1$	$\lvert a^-\rvert > 1$
Partial pass band	$4P^- < \Omega < 4P^+$	$\lvert a^+\rvert < 1$	$\lvert a^-\rvert > 1$
Stop band	$4P^+ < \Omega$	$\lvert a^+\rvert < 1$	$\lvert a^-\rvert < 1$

It is also noted that there are singularities in $a^\pm$ at $\Omega = 2P^\mp$. Typical behaviour of $|a^\pm|$ as a function of Ω is shown in Fig. **??** for $\alpha = 0.4$ and $c = 0.6$. For these values, the band boundaries $\Omega = 4P^\pm(\alpha,c)$ occur at $\Omega = 2.05$ and $\Omega = 5.56$.

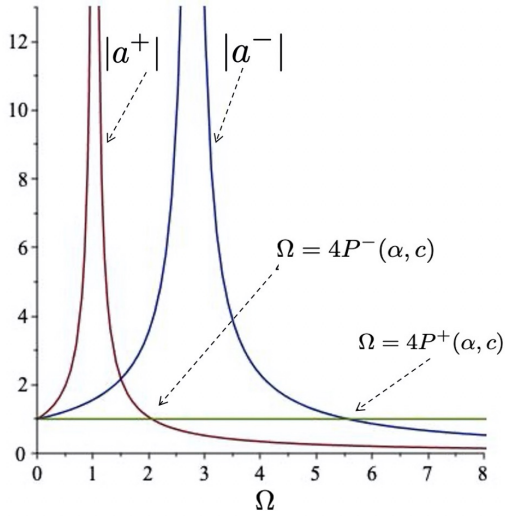

Figure 5: The functions $|a^\pm(\Omega)|$ for $\alpha = 0.4$ and $c = 0.6$. The singularities of $a^\pm$ correspond to the values of Ω, where $\lambda^\pm$ vanish. The band boundaries $\Omega = 4P^\pm(\alpha,c)$ occur at $\Omega = 2.05$ and $\Omega = 5.56$.

3.2.1 Stop-band

When the forcing frequency is in the stop band, we have $|a^\pm| < 1$, and hence the components of Green's matrix are exponentially localised (compare with [**?**]).

In this case, the function $F(n,\Omega,\alpha,c)$, defined by (**??**) and (**??**), may be written as

$$F(n,\Omega,\alpha,c)=\frac{1}{2\Omega(1-\alpha^2)(P^-(\alpha,c)-P^+(\alpha,c))}\left[\frac{a^-}{\sqrt{1-(a^-)^2}}\left(\frac{1-\sqrt{1-(a^-)^2}}{a^-}\right)^{|n|}\right.$$
$$\left.-\frac{a^+}{\sqrt{1-(a^+)^2}}\left(\frac{1-\sqrt{1-(a^+)^2}}{a^+}\right)^{|n|}\right]. \quad (31)$$

3.2.2 Partial pass band

In this region, $|a^-|>1$ and $|a^+|<1$. This regime is a special feature of the wave motion in a chiral elastic chain. For the one-dimensional motion of a chain without chirality, such a regime is not observed (see [**?**]).

The "-" integral in (**??**) warrants further consideration as this form appears in the function $F(n,\Omega,\alpha,c)$ in both the partial and total pass bands. In order to evaluate the "-" integral, this may be done by transforming to a suitable contour integral. The contour integral used may have a path around the unit circle or along a rectangular contour in the upper half of the complex plane with corners $(-\pi,0),(\pi,0),(\pi,\pi+i\infty),(-\pi,-\pi+i\infty)$. In both case the poles lie on the contour itself. These solutions are oscillatory and, in order to impose the radiation condition, regularisation is needed in both methods. This results in one pole being moved inside the contour and one pole being moved outside. Only the pole inside the contour contributes to the contour integral leading to a result which obeys the radiation condition. Thus, taking into account the radiation condition at infinity, we can represent the function $F(n,\Omega,\alpha,c)$ in the partial pass band as

$$F(n,\Omega,\alpha,c) = \frac{1}{2\Omega(1-\alpha^2)(P^-(\alpha,c)-P^+(\alpha,c))}\left[\frac{ie^{i|n|\theta^-}}{\sin\theta^-} - \frac{a^+}{\sqrt{1-(a^+)^2}}\left(\frac{1-\sqrt{1-(a^+)^2}}{a^+}\right)^{|n|}\right], \quad (32)$$

where

$$\cos\theta^{\pm}=\lambda^{\pm}. \quad (33)$$

The first term in (**??**) represents the propagating solution, obeying the radiation condition at infinity, and the second term in (**??**) represents the evanescent solution.

3.2.3 Total pass band

In this regime, $|a^{\pm}|>1$ and both "$\pm$" integrals in (**??**) lead to oscillatory solutions. The function $F(n,\Omega,\alpha,c)$, incorporating the radiation condition, is given in the total pass band by

$$F(n,\Omega,\alpha,c)=\frac{1}{2\Omega(1-\alpha^2)(P^-(\alpha,c)-P^+(\alpha,c))}\left[\frac{ie^{i|n|\theta^-}}{\sin\theta^-}-\frac{ie^{i|n|\theta^+}}{\sin\theta^+}\right]. \quad (34)$$

We note that other formal solutions of (**??**) can be obtained by adding a Floquet-Bloch wave to (**??**), but they will not necessarily satisfy the radiation conditions.

The dimensionless time-harmonic displacements $\mathbf{u}_{\pm}^{(n)}$ are then given by (**??**).

3.3 Motion of the nodal points

The trajectory of node n is determined by $\mathbf{U}^{(n)}$. It is an ellipse of the form

$$\mathbf{x}^{(n)T}\mathbf{M}^{(n)}\mathbf{x}^{(n)} = 1, \tag{35}$$

with a positive definite matrix $\mathbf{M}^{(n)}$ given by

$$\mathbf{M}^{(n)} = \frac{1}{\Delta^2}\begin{pmatrix} \mathrm{Re}(U_2^{(n)})^2 + \mathrm{Im}(U_2^{(n)})^2 & -\mathrm{Re}(U_1^{(n)})\mathrm{Re}(U_2^{(n)}) - \mathrm{Im}(U_1^{(n)})\mathrm{Im}(U_2^{(n)}) \\ -\mathrm{Re}(U_1^{(n)})\mathrm{Re}(U_2^{(n)}) - \mathrm{Im}(U_1^{(n)})\mathrm{Im}(U_2^{(n)}) & \mathrm{Re}(U_1^{(n)})^2 + \mathrm{Im}(U_1^{(n)})^2 \end{pmatrix}, \tag{36}$$

where

$$\Delta = \mathrm{Re}(U_1^{(n)})\mathrm{Im}(U_2^{(n)}) - \mathrm{Re}(U_1^{(n)})\mathrm{Im}(U_2^{(n)}), \tag{37}$$

and $\mathbf{x}^{(n)}$ are the local coordinates associated with the centre of the ellipse n and aligned perpendicular and parallel to the chain (see [**?**], [**?**] for a similar matrix).

The major and minor axes of the ellipse are determined in magnitude and direction by the eigenvalues and eigenvectors of $\mathbf{M}^{(n)}$.

3.4 Decay rate in the stop band

For evanescent waves, when the forcing frequency is in the stop-band interval, their amplitude will decay as they travel away from the forced central node. As n increases, the "-" function in (**??**) will dominate the "+" function (also see Fig. **??**). Let $L(\Omega, \alpha, c)$ be defined as

$$L(\Omega, \alpha, c) = \lim_{n\to\infty} \frac{F(n+1, \Omega, \alpha, c)}{F(n, \Omega, \alpha, c)} \tag{38}$$

Using (**??**), this becomes

$$L(\Omega, \alpha, c) = \left(\frac{1 - \sqrt{1 - (a^-)^2}}{a^-}\right), \tag{39}$$

allowing the asymptotic form of the Green's matrix $G^{(\infty)}$ to be written as

$$G^{(\infty)} = \begin{pmatrix} (2c - \Omega) - c(L + L^{-1}) & i\alpha\Omega \\ -i\alpha\Omega & (2 - \Omega) - L - L^{-1} \end{pmatrix} F(n, \Omega, \alpha, c). \tag{40}$$

For a unit applied force, the elements of the matrix $\mathbf{M}^{(n)}$ are related directly to the elements of $G^{(\infty)}$ as $\mathrm{Re}(U_1^{(n)}) = G_{11}^{(\infty)}$, $\mathrm{Im}(U_1^{(n)}) = G_{12}^{(\infty)}$, $\mathrm{Re}(U_2^{(n)}) = G_{22}^{(\infty)}$ and $\mathrm{Im}(U_2^{(n)}) = G_{21}^{(\infty)}$.

As n increases, we note that the off-diagonal elements in the matrix $\mathbf{M}^{(n)}$ become much smaller relative to the diagonal elements, and hence the elliptical trajectories of the nodal points get their axes aligned parallel and perpendicular to the chain.

As a measure of decay rate, the ratio of the lengths of the major axes of successive ellipses will be used. The lengths of the major and minor axes are related to the eigenvalues of the matrix $\mathbf{M}^{(n)}$. Because of the separable nature of $G^{(\infty)}$, the dependence on n appears only through the function $F(n, \Omega, \alpha, c)$. The decay rate becomes constant with respect to n as $n \to \infty$ and is given by $L(\Omega, \alpha, c)$ in (**??**).

3.5 An illustrative example for the case of existing pre-tension

Consider an example with the following dimensionless parameter values: $\alpha = 0.3,\ c = 0.8,$

$f_1 = 1,\ f_2 = 8$. The dispersion diagram, presenting ω versus k, is shown in Fig. **??**. Given that $\Omega = \omega^2$, the stop band consists of all frequencies such that $\Omega > 5.215$; the partial pass band is $2.70 < \Omega < 5.215$; the total pass band is $\Omega < 2.70$. Hence, three representative forcing frequencies will be chosen, one in each band. The trajectories of the negatively labelled nodes are identical to the corresponding positively labelled nodes. The nodal trajectories for each case (b) $\Omega = 6$, (c) $\Omega = 2.8$ and (d) $\Omega = 1$ are shown in Figs **??**, **??** and **??** for the stop band, partial pass band and total pass band respectively.

In Fig. **??** and for $n = 0$, the largest trajectory is influenced by the application of the force, although it should be noted that the major axis of this elliptical trajectory is not exactly aligned with the direction of the force. In fact, the major axis of the $n = 0$ ellipse and the applied force make angles of 80.3° and 82.9° with the positive x_1-axis respectively. The trajectory is determined by a combination of dimensionless parameters, α, c and $(f_1, f_2)^T$. As $|n|$ increases, major axis directions align with the direction of the chain and the eccentricities for trajectories of neighbouring nodal points approach the same limit. In addition, for $|n|$ sufficiently large, the major axes decrease by a factor of 0.47 in neighbouring ellipses for this set of parameters.

In the partial pass band and in the total pass band, the trajectories are shown in Fig. **??** and Fig. **??**, respectively. It is noted that in the total pass band the major axis of the $n = 0$ ellipse makes an angle of 83.9° with the positive x_1-axis.

4 Chirality for an asymmetrically localised Green's matrix

A special regime for the chiral chain is the regime of the "partial pass band" frequencies, as discussed in Section **??**, where Green's matrix (**??**) is associated with propagating waves in addition to evanescent waves, as shown in (**??**). Formally one can add to (**??**) an appropriately normalised Floquet-Bloch wave, propagating in the negative direction along the chain, to obtain a new "one-sided" Green's matrix (**??**), where $F(n, \Omega, \alpha, c)$ is replaced by $F_A(n, \Omega, \alpha, c)$:

$$F_A(n,\Omega,\alpha,c) = \frac{1}{2\Omega(1-\alpha^2)(P^-(\alpha,c)-P^+(\alpha,c))}\left[\frac{-2\sin(n\theta^-)}{\sin\theta^-}H(n) - \frac{a^+}{\sqrt{1-(a^+)^2}}\left(\frac{1-\sqrt{1-(a^+)^2}}{a^+}\right)^{|n|}\right]. \quad (41)$$

Here $H(n)$ is the Heaviside function, and θ^- is given in (**??**). Such a Green's matrix remains non-zero along the entire chain, but it has an incoming wave towards the origin and outgoing wave from the origin for positive values of n, and it is exponentially localised for negative n. The one-sided Green's matrix may be used effectively for the description of localised defect modes in semi-infinite chiral chains. The fact that $F_A(n, \Omega, \alpha, c)$ is purely real is significant, as discussed below.

4.1 Illustrative example

An illustrative numerical example is given in Fig. **??**. Here, in the first part, shown in Fig. **??**, the resulting trajectories of the infinite chiral chain may be seen when a time-harmonic force, with amplitude vector $(f_1, f_2) = (2, 6)$, is applied to the central $(n = 0)$ node. The vortex or circular component of the elliptical motion may be seen in Fig. **??**. This component is introduced and discussed in [**?**] and [**?**]. The corresponding videos may be seen in the supplementary material. For nodes $n > 0$, an evanescent wave is coupled with a standing wave; the latter only being present for large values of n. For $n \leq 0$, the only term left in $F_A(n, \Omega, \alpha, c)$, given in (**??**), is the second term in the brackets. Thus $F_A(n, \Omega, \alpha, c)$ is purely real and this leads to the off-diagonal elements

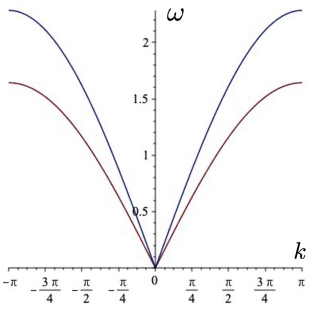

(a) Dispersion diagram: ω versus k for a chiral chain; $\omega^2 = \Omega$.

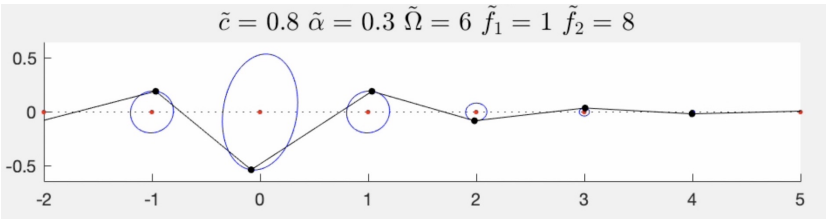

(b) Stop band $\Omega = 6$

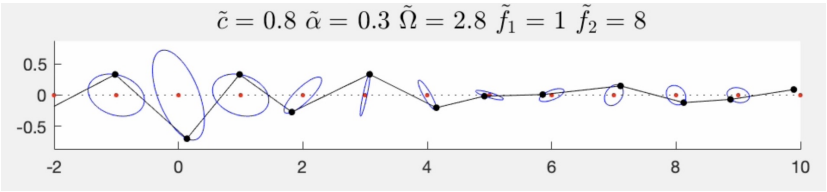

(c) Partial pass band $\Omega = 2.8$

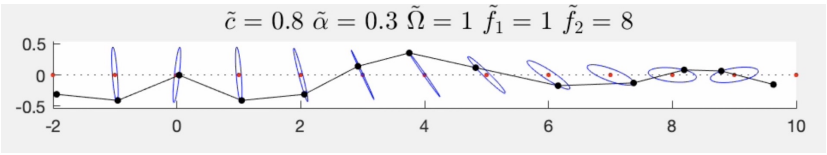

(d) Total pass band $\Omega = 1$

Figure 6: The dispersion diagram (a) and the elliptical trajectories for an infinite chiral chain with pre-tension, when the central node ($n = 0$) is forced in a time-harmonic manner with force amplitude $(f_1, f_2) = (1, 8)$. The forcing frequency is chosen from (b) the stop band $\Omega = 6$, (c) the partial pass band $\Omega = 2.8$ and (d) the total pass band $\Omega = 1$. Parameter values: $\alpha = 0.3,\ c = 0.8$.

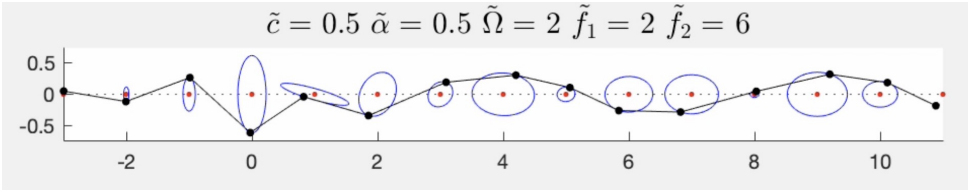

(a) The full motion of the nodes

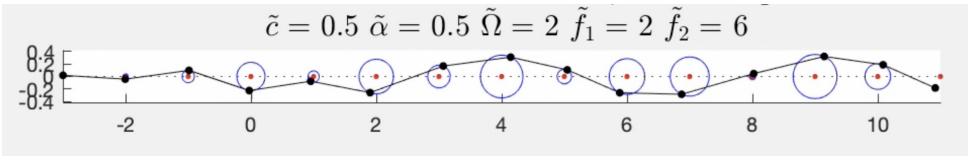

(b) The circular component of the motion of the nodes

Figure 7: The infinite chiral chain with the central ($n = 0$) node forced by a time-harmonic force of amplitude vector $(f_1, f_2) = (2, 6)$. The 'one-sided' Green's matrix has been used. Parameter values are: $\alpha = 0.5, c = 0.5, \Omega = 2$.

in the matrix $\mathbf{M}^{(n)}$ in (**??**) having the form $-f_1 f_2 \det\big(G^{(n)}\big)$ with $\det\big(G^{(n)}\big) = 0$. This shows that for $n \leq 0$, the ellipses are orientated with their axes along and perpendicular to the chain which may be counter-intuitive for the forced node. In addition, for large positive values of n, there is only the single propagating term in the function $F_A(n, \Omega, \alpha, c)$ given in (**??**) and, because this is purely real, the off-diagonal terms are again given by $-f_1 f_2 \det\big(G^{(n)}\big)$ with $\det\big(G^{(n)}\big) \to 0$ as $n \to \infty$. Hence the ellipses for large positive values of n are aligned with axes perpendicular and parallel to the chain. For low positive values of n, both terms in the brackets in (**??**) contribute, resulting in a more general alignment of the axes of the ellipses.

5 Dynamic degeneracy

An important special case of the problem discussed in section **??** is one where there is no transverse pre-tension ($c = 0$) in the infinite chiral chain. The eigenvalue problem has been discussed in section **??** and the governing equations, in dimensionless variables, for the case with a time-harmonic force acting on the central node, are given by (**??**), with $c = 0$.

5.1 Green's function for a lattice with no transverse pre-tension

When $c = 0$, there is only one non-zero root of the dispersion equation (**??**). In this case, two regimes are observed: the pass band for $0 < \Omega \leq 4/(1 - \alpha^2)$, and the stop band for $\Omega > 4/(1 - \alpha^2)$. It is convenient to introduce an analogous function to $F(n, \Omega, \alpha, 0)$ with a modified dispersion equation showing the one non-zero root. Hence let

$$I(n, \Omega, \alpha) = \frac{1}{2\pi} \int_{-\pi}^{\pi} \frac{e^{ikn}}{2(1 - \cos k) - (1 - \alpha^2)\Omega}\, dk. \tag{42}$$

The Green's matrix is then

$$G^{(n)} = \begin{pmatrix} I(n, \Omega, \alpha) & -i\alpha I(n, \Omega, \alpha) \\ i\alpha I(n, \Omega, \alpha) & \frac{(\Omega-2)}{\Omega} I(n, \Omega, \alpha) + \frac{I(n+1, \Omega, \alpha)}{\Omega} + \frac{I(n-1, \Omega, \alpha)}{\Omega} \end{pmatrix}. \tag{43}$$

In the *stop band* we have $\Omega > 4/(1-\alpha^2)$, and

$$I(n,\Omega,\alpha) = \frac{-2^{-|n|}\left(2-(1-\alpha^2)\Omega + \sqrt{(1-\alpha^2)\Omega\big[(1-\alpha^2)\Omega-4\big]}\right)^{|n|}}{\sqrt{(1-\alpha^2)\Omega\big[(1-\alpha^2)\Omega-4\big]}}, \tag{44}$$

is exponentially localised as a function of n.

On the other hand, in the *pass band* $0 < \Omega \leq 4/(1-\alpha^2)$, and

$$I(n,\Omega,\alpha) = \frac{ie^{i|n|\theta_1}}{2\sin\theta_1}, \tag{45}$$

where

$$\cos\theta_1 = \frac{2-(1-\alpha^2)\Omega}{2}. \tag{46}$$

5.2 Green's matrix in the stop band with no transverse pre-tension

Here the forcing frequency is required to be in the regime $\Omega > 4/(1-\alpha^2)$. This results in exponential solutions given in (**??**).

For the form of $I(n,\Omega,\alpha)$ in the stop band, a recurrence relation may be used to simplify the Green's matrix element $G_{22}^{(n)}$ in (**??**). For all $n > 0$ the simplification is the same but the case $n = 0$ is unique. This leads to

$$G^{(n)} = \begin{bmatrix} 1 & -i\alpha \\ i\alpha & \Lambda^{(n)}(\Omega,\alpha) \end{bmatrix} I(n,\Omega,\alpha), \tag{47}$$

where

$$\Lambda^{(n)}(\Omega,\alpha) = \begin{cases} \alpha^2 + \sqrt{\frac{(1-\alpha^2)\left(\Omega(1-\alpha^2)-4\right)}{\Omega}}, & n = 0 \\ \alpha^2, & n \neq 0 \end{cases} \tag{48}$$

The form of $\Lambda^{(n)}(\Omega,\alpha)$ shows that there is an intrinsic difference in behaviour between the central, forced node and the other nodes in addition to the effect that the magnitude and direction of the forcing vector has on the motion. The dimensionless time-harmonic displacements $\mathbf{u}^{(n)}$ are then given by $\mathbf{u}^{(n)} = \mathrm{Re}\Big(\mathbf{U}^{(n)}e^{i\omega t}\Big)$, where the time-harmonic amplitude $\mathbf{U}^{(n)}$ is given in (**??**). Using (**??**), (**??**), (**??**) and (**??**) gives the characterising matrix $\mathbf{M}^{(n)}$ for the ellipse as

$$\mathbf{M}^{(n)} = \frac{1}{(f_1^2+\Lambda^{(n)}f_2^2)^2\alpha^2 I(n,\Omega,\alpha)^2}\begin{pmatrix} \alpha^2 f_1^2 + \Lambda^{(n)2}f_2^2 & (\alpha^2-\Lambda^{(n)2})f_1f_2 \\ (\alpha^2-\Lambda^{(n)2})f_1f_2 & f_1^2+\alpha^2 f_2^2 \end{pmatrix}. \tag{49}$$

For this case of no existing transverse pre-tension, the geometry of the elliptical motions of the nodes is governed by the matrix $\mathbf{M}^{(n)}$ (**??**). Consider the orientation of the ellipses. The off-diagonal elements of this matrix are zero if either $f_1 = 0$ or $f_2 = 0$ or $\Lambda^{(0)} = \alpha^2$. Thus by linearity, the general loading case will always result in the unforced nodes having the axes of their elliptical trajectories oriented along or perpendicular to the chain. It may also be seen that for the unforced nodes, $M_{11}^{(n)} < M_{22}^{(n)}$ and hence the major axes of the trajectories of

these nodes will be aligned with the chain. For the forced node, (**??**) and (**??**) show that $\Lambda^{(0)} = \alpha^2$ only at the limiting point $\alpha = 1$ or when the forcing frequency is on the edge of the stop band. Thus for the general loading case with no transverse pre-tension, the ellipse of the forced node will in general not have an axis aligned to the chain unless the loading is either case $f_1 = 0$ or $f_2 = 0$. As these two loading cases form a basis for the general loading, these will be examined in detail.

5.2.1 The case of a loading along the chain, ($f_2 = 0$)

Here

$$\mathbf{M}^{(n)} = \frac{1}{f_1^2 I(n,\Omega,\alpha)^2} \begin{pmatrix} 1 & 0 \\ 0 & 1/\alpha^2 \end{pmatrix}, \tag{50}$$

and the equations of the trajectories of the nodes are

$$\alpha^2 {x_1^{(n)}}^2 + {x_2^{(n)}}^2 = \alpha^2 f_1^2 I(n,\Omega,\alpha)^2, \tag{51}$$

i.e. all ellipses with their major axes aligned with the chain (since $\alpha < 1$). All ellipses have the same eccentricity. The decay factor of the lengths of the major axes of the ellipses as n increases is independent of n and given by

$$\left| \frac{I(n+1,\Omega,\alpha)}{I(n,\Omega,\alpha)} \right| = \left| \frac{(1-\alpha^2)\Omega - 2 - \sqrt{(1-\alpha^2)\Omega\left[(1-\alpha^2)\Omega - 4\right]}}{2} \right|. \tag{52}$$

It is also seen (**??**) that the eccentricity depends only on α and not on Ω. Hence ellipses of the same eccentricity will be found for all values of the forcing frequency (in the stop band).

5.2.2 The case of a loading perpendicular to the chain, ($f_1 = 0$)

Here

$$\mathbf{M}^{(n)} = \frac{1}{f_2^2 I(n,\Omega,\alpha)^2} \begin{pmatrix} 1/\alpha^2 & 0 \\ 0 & 1/\Lambda^{(n)2} \end{pmatrix}, \tag{53}$$

and the equations of the nodal trajectories are

$$\left(\frac{x_1^{(n)}}{\alpha} \right)^2 + \left(\frac{x_2^{(n)}}{\Lambda^{(n)}} \right)^2 = f_2^2 I(n,\Omega,\alpha)^2. \tag{54}$$

At the forced node ($n = 0$), using $\Lambda^{(0)} > \alpha$ (see (**??**)) and (**??**)), we observe that the elliptical trajectory will have its major axis oriented perpendicular to the chain. For all other nodes, their major axes will be oriented along the chain. This stark change in behaviour occurs since, for this case of no transverse pre-tension, there is no component of the connector force perpendicular to the chain. The only external force acting perpendicular to the chain is f_2 and it acts only at the central ($n = 0$) node. For the unforced nodes, the decay factor of the lengths of the major axes in this case will again be given by (**??**). It is of note that the common eccentricity of the unforced nodes is also the same as in that of the unforced nodes in case discussed in section **??**.

It is further noted that, by linearity, the solution to the problem for a general loading force vector in the case of no transverse pre-tension is a linear combination of cases discussed here and in section **??**. Hence, the solution to any general loading problem would lead to the unforced nodes having their trajectories with the major axes

in the direction of the chain with a decay factor given by (**??**). The motion of the central node in general would be elliptical with axes not generally aligned parallel or perpendicular to the chain.

It is also observed that, for the elliptical motion of the unforced nodes ($n \neq 0$), the eccentricity depends only on α and not on Ω. Hence ellipses of the same eccentricity will be found for all values of the forcing frequency (in the stop band). The eccentricity of the ellipse, corresponding to the forced node ($n = 0$), depends on both α and Ω. Essentially, this is a consequence of the definition of $\Lambda^{(n)}$ (see (**??**)).

The decay factor given in (**??**) is shown in Fig. **??** as a function of α and Ω for values of Ω in the stop band ($\Omega > 4/(1-\alpha^2)$). The decay factor increases with increasing chirality α for fixed Ω and decreases with increasing forcing frequency Ω for fixed α.

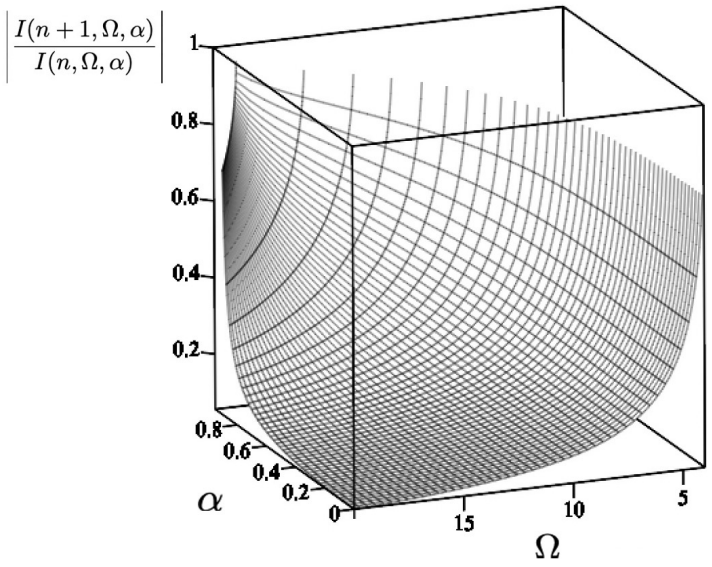

Figure 8: The decay factor $\left|\frac{I(n+1,\Omega,\alpha)}{I(n,\Omega,\alpha)}\right|$ for the major axes of the ellipses in the case when there is no transverse pre-tension in the chain.

5.3 Green's matrix in the pass band with no transverse pre-tension

The Green's matrix is given in equations (**??**) and (**??**). For the form of the function $I(n, \Omega, \alpha)$ in (**??**), it may be shown that the Green's matrix also simplifies to the form in equations (**??**) and (**??**) and hence the geometries of the nodal trajectories are determined from (**??**). Apart from the central ($n = 0$) node, all the other nodes have elliptical trajectories which align such that their major axes are parallel to the chain and they are all identical in size, eccentricity and alignment. Of course, neighbouring nodes will have a phase difference.

5.4 An illustrative example for the case of no transverse pre-tension

Consider an example with the same chirality parameter value as was used in the example in section **??**. Choose $c = 0,\ \alpha = 0.3,\ f_1 = 1,\ f_2 = 1$. The dispersion diagram, presenting a single curve ω versus k for a chiral chain where $c = 0$, is shown in Fig. **??**. There is only one mode with non-zero frequency and the stop band consists of all frequencies such that $\omega^2 = \Omega > 4.396$. Let us choose a representative forcing frequency from the stop band and let it be $\Omega = 5$. The trajectories of the negatively labelled nodes are identical to the corresponding positively labelled nodes. The nodal trajectories $n = -1$ to $n = 4$ are shown in Fig. **??**.

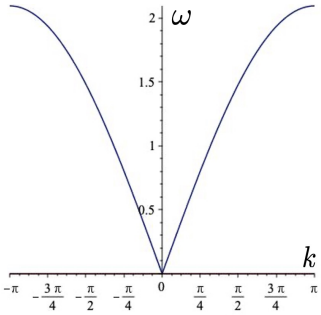

(a) Dispersion diagram: ω versus k for a chiral chain with no transverse pretension; $\omega^2 = \Omega$.

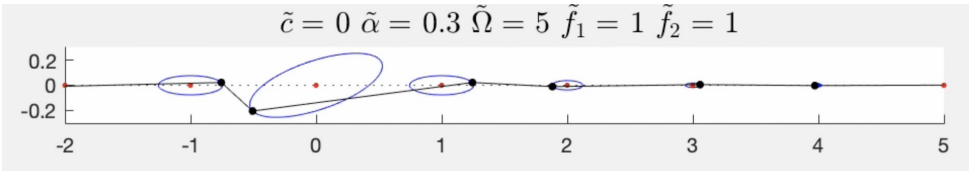

(b) Forcing frequency in the stop band, $\Omega = 5$.

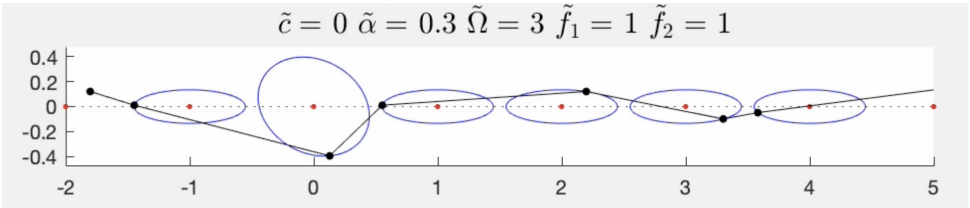

(c) Forcing frequency in the pass band, $\Omega = 3$.

Figure 9: The dispersion diagram (a) for waves in a chiral chain with no transverse pretension shows a single dispersion curve. The resulting elliptical trajectories are shown for an infinite chiral chain with no transverse pre-tension, when the central node ($n = 0$) is forced in a time-harmonic manner with force amplitude (f1, f2) = (1, 1). The chirality parameter $\alpha = 0.3$. The forcing frequencies are chosen to be from (b) the stop band $\Omega = 5$, and (c) the pass band $\Omega = 3$.

It may be seen that all the unforced nodes are aligned to the chain as expected. For $n = 0$, the shape and orientation of the elliptical trajectory are influenced by the application of the force. The major axis of the $n = 0$ ellipse and the applied force make angles of 18.6° and 45° with the positive x_1-axis respectively. For $|n|$ sufficiently large, the major axes of the (similar) ellipses decreases by a factor of 0.48 in neighbouring ellipses.

Now choose a representative forcing frequency in the pass band and let it be $\Omega = 3$, keeping the other parameters unchanged in value. The results are shown in Fig. **??**. All unforced ellipses are aligned to the chain with no decay as expected.

6 Exponentially localised chiral defect modes

Consider the one-dimensional infinite chain, of inter-nodal spacing a, with gyroscopic spinners attached to the nodes as before but with the central ($n = 0$) being perturbed translationally and rotationally. This is achieved with the central node having a mass $m + M$ and a spinner constant $\alpha + A$. The general case of existing pre-tension in the lattice is considered and time-harmonic solutions for the displacement of the nodes caused by this

defect in the central node are sought. The governing equations for the amplitude $\mathbf{U}^{(n)}$ of the time-harmonic displacement of node n are

$$\begin{aligned} -(m+M\delta_{n0})\omega^2 U_1^{(n)} &= c_1(U_1^{(n+1)}+U_1^{(n-1)}-2U_1^{(n)})+i(\alpha+A\delta_{n0})\omega^2 U_2^{(n)}, \\ -(m+M\delta_{n0})\omega^2 U_2^{(n)} &= c_2(U_2^{(n+1)}+U_2^{(n-1)}-2U_2^{(n)})-i(\alpha+A\delta_{n0})\omega^2 U_1^{(n)}. \end{aligned} \tag{55}$$

Introduce the dimensionless variables defined in (**??**) together with the following:

$$\tilde{M}=\frac{M}{m}, \quad \tilde{A}=\frac{A}{\alpha}, \tag{56}$$

where the quantities with the symbol "$\sim$" are dimensionless. Equations (**??**) become (dropping the "$\sim$" for convenience)

$$\begin{aligned} -\Omega U_1^{(n)} &= U_1^{(n+1)}+U_1^{(n-1)}-2U_1^{(n)}+i\alpha\Omega U_2^{(n)}+(MU_1^{(n)}+i\alpha A U_2^{(n)})\Omega\delta_{n0}, \\ -\Omega U_2^{(n)} &= c(U_2^{(n+1)}+U_2^{(n-1)}-2U_2^{(n)})-i\alpha\Omega U_1^{(n)}+(MU_2^{(n)}-i\alpha A U_1^{(n)})\Omega\delta_{n0}. \end{aligned} \tag{57}$$

Here $\Omega=\omega^2$. This system may be interpreted as a forced system, as in (**??**), with translational and rotational inertia forces on the central node

$$\tilde{\mathbf{f}}=\Omega(M\mathbf{I}+i\alpha A\mathbf{R})\mathbf{U}^{(0)}. \tag{58}$$

Using these forces with (**??**) leads to

$$\Big(\mathbf{I}-\Omega G^{(0)}(M\mathbf{I}+i\alpha A\mathbf{R})\Big)\mathbf{U}^{(0)}=\mathbf{0}. \tag{59}$$

For non-zero solutions of (**??**), it is required that

$$\begin{aligned} &\Big(2\Omega M\det\Big(G^{(0)}\Big)-\mathrm{Tr}(G^{(0)})\Big)^2-4\Big(\alpha\Omega A\det\Big(G^{(0)}\Big)+\mathrm{Im}(G_{12}^{(0)})\Big)^2 \\ &\qquad =\mathrm{Tr}(G^{(0)})^2+(G_{12}^{(0)}-G_{21}^{(0)})^2-4\det\Big(G^{(0)}\Big), \end{aligned} \tag{60}$$

where $G^{(n)}$ is given in (**??**). Equation (**??**) represents a hyperbola in the space of perturbed mass and spinner constant (A,M). It has asymptotes with equations

$$M=\pm\alpha A+\frac{\mathrm{Tr}(G^{(0)})\pm 2\,\mathrm{Im}(G_{12}^{(0)})}{2\Omega\det\big(G^{(0)}\big)}. \tag{61}$$

The asymptotes intersect at the point

$$(A^*,M^*)=\Big(-\mathrm{Im}(G_{12}^{(0)})/(\alpha\Omega\ \det(G^{(0)})),\mathrm{Tr}(G^{(0)})/(2\Omega\ \det(G^{(0)}))\Big).$$

The hyperbola (**??**) represents the values of the perturbation pairs (A,M) which support time-harmonic waves in the chain. The amplitude $\mathbf{U}^{(0)}$ is determined from (**??**), with the other amplitudes $\mathbf{U}^{(n)}$ $(n>0)$ found from (**??**) and hence they depend on the Green's matrix for the chain with pre-tension. This will lead to three regimes

for the frequency of such waves with dispersion properties determined according to (??)-(??) as discussed in section ??.

For a given chain with given dimensionless spinner constant, α, and dimensionless stiffness ratio, c, the frequency may be chosen in one of the three regimes according to (??), (??). The resulting hyperbola (??) will give "acceptable" perturbation pairs (A, M) such that waves (fully propagating or evanescent depending on the value of the frequency chosen) are supported. The displacement amplitudes, and hence the nodal trajectories, may be found from (??) with $\mathbf{U}^{(0)}$ being the non-zero solution of (??).

6.1 An illustrative example of defect modes in the stop band

Consider an illustrative example with parameter values as follows: $\alpha = 0.4,\ c = 0.2$. The stop band of the periodic system consists of all frequencies such that $\Omega > 4.94$. For this illustration, choose $\Omega = 6$. The resulting hyperbola in the (A, M) plane is shown in Fig. ??. This hyperbola also depends on Ω and this is shown in Fig. ?? for values of Ω in the stop band. From Fig. ??, it will be seen that Ω has only a small influence on the hyperbola in the (A, M) plane. The direction of the asymptotes depends only on α and not on the frequency $\omega = \sqrt{\Omega}$ of the waves.

Choose a perturbation of the central node, $A = 0.5$. For this value of A, the two allowable perturbations for the mass of the central node are $M = -0.09$ and $M = -1.375$.

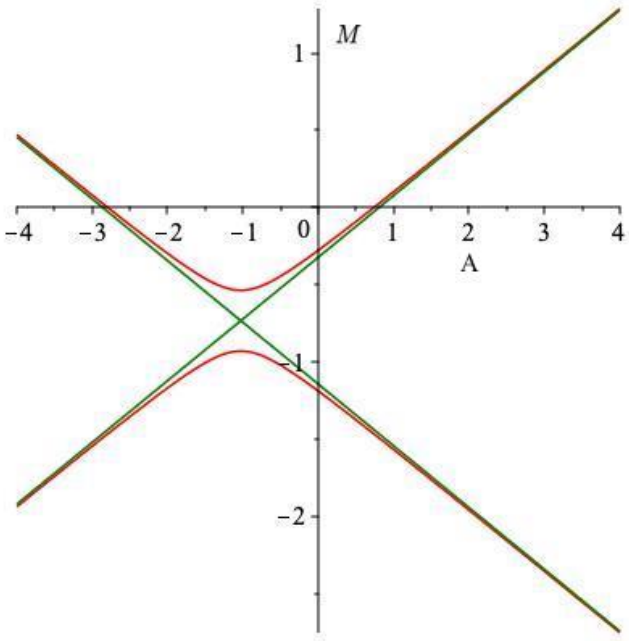

Figure 10: The hyperbola, together with its asymptotes, indicating acceptable defect pairs (A, M) for $\alpha = 0.4,\ c = 0.2,\ \Omega = 6$

(i) (A, M)=(0.5,-0.09)

Using the stop band Green's matrix (??) and (??), the $n = 0$ node displacement amplitude of the central node may be found from (??) and is given by $\mathbf{U}^{(0)} = (1, 0.728i)^T$. Since the components of $\mathbf{U}^{(0)}$ are purely real and purely imaginary respectively, the axes of the elliptical trajectory of the central node are aligned parallel and perpendicular to the chain. This statement about the alignment of the axes applies to all the nodes. Consider the decay rate as measured by the size of the ratio of the major axes of neighbouring nodes. This will be $|\frac{\mathrm{Re}(U_1^{(n+1)})}{\mathrm{Re}(U_1^{(n)})}|$ which settles after the first few nodes to a constant value of 0.409. The trajectories of the first four nodes $(n = 0, .., 3)$ are nested for convenience and for comparison. These are shown in Fig. ??a.

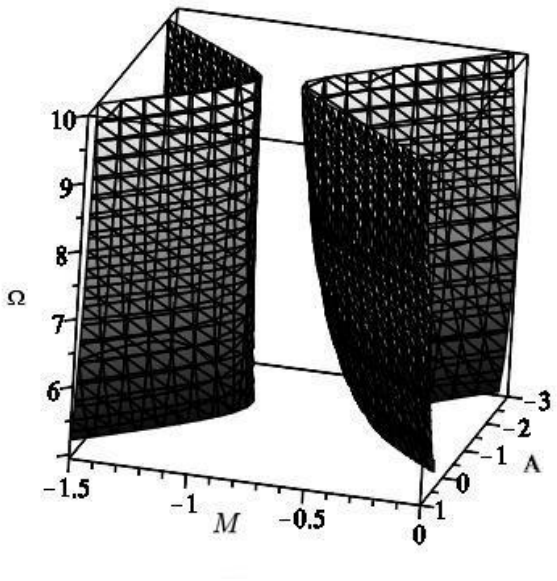

Figure 11: The (A, M, Ω) space of acceptable values of perturbations for $\alpha = 0.4,\ c = 0.2$

(ii) (A, M)=(0.5,-1.375)

We note that the negative translational inertia $M + m$ is admissible by the present model; in the physical configuration, this would imply a presence of a spring-mass resonator. Using the stop band Green's matrix (**??**) and (**??**), the $n = 0$ node displacement amplitude of the central node may be found from (**??**) and is given by $\mathbf{U}^{(0)} = (1, -1.373i)^T$. Since the components of $\mathbf{U}^{(0)}$ are again purely real and purely imaginary respectively, the axes of the elliptical trajectory of the central node are aligned parallel and perpendicular to the chain. Again, from the components of $\mathbf{U}^{(n)}$ for all n are purely real and purely imaginary, indicating that this type of alignment applies to all nodes. The rate of decay is again taken as $|\frac{\mathrm{Re}(U_1^{(n+1)})}{\mathrm{Re}(U_1^{(n)})}|$ and again has the value of 0.409. The nested trajectories of the first four nodes ($n = 0..3$) are shown in Fig. **??**. It is noted that in this mode the major axis of the central ($n = 0$) node is aligned perpendicular to the chain

7 Concluding remarks

In this paper, fundamentals of the dynamics of elastic chiral systems have been shown together with an analytical description of chiral elastic waves, including dynamic Green's matrices, in a closed analytical form. The theory, as presented, has covered chiral Floquet-Bloch elastic waves in addition to forced vibrations and exponentially localised waveforms, which may be referred to as chiral dynamic defect modes.

Several new concepts of waveforms in chiral lattice systems have been introduced and accompanied by demonstrations for coupled non-degenerate and degenerate chiral motions. These include chiral dynamic coupling, dynamic degeneracy, chiral wave forms associated with the partial pass bands frequencies, Floquet-Bloch waves versus forced vibrations, and exponentially localised chiral wave forms corresponding to perturbations of the inertial properties of the lattice. The generality of these concepts makes them applicable to a wide range of physical settings of elastic chiral lattice systems.

A dynamic response of a one-dimensional *chiral* elastic chain has been analysed, where the motion of every nodal point within the chain is associated with the motion of a gyroscope, which provides a chiral coupling

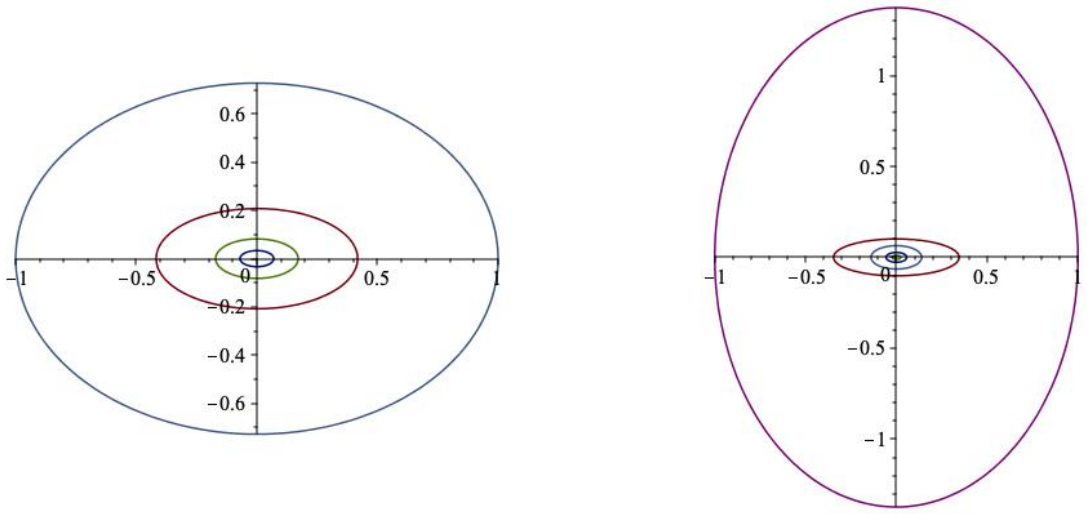

(a) The mode (A, M)=(0.5,-0.09)

(b) The mode (A, M)=(0.5,-1.375)

Figure 12: The (nested) trajectories of the first four nodes ($n = 0, ..., 3$). $\alpha = 0.4,\ c = 0.2,\ \Omega = 6$. It is noted that $(m+M)/m > 0$ in the case (a), and $(m + M)/m < 0$ in the case (b).

between the longitudinal and transverse displacements. This leads to a vector problem of wave propagation in a one-dimensional chain and, in addition, the dispersion relations possess a special regime, referred to as the *partial pass band*, where both exponentially localised waveforms and propagating waves can be observed.

Additionally, by introducing a pre-tension into such an elastic chain, one can formally remove a degeneracy, which is expected and observed in the case of two-dimensional wave forms in a standard one-dimensional lattice. Detailed analysis [**?**] introduced the notion of vortex waves in two-dimensional triangular chiral lattices. As demonstrated in the present paper, chain pre-tension appears to be useful, and the concept may be extended to chiral lattices of higher dimensions.

The dynamic Green's matrix is a fundamental object of interest in this problem, and it has been presented in a closed analytical form in full generality. This analysis has enabled the identification of regimes of wave localisation in addition to the conventional propagating modes. While observing the effect of chirality in a special representation of the eigenvectors for Floquet-Bloch waves, we have also identified the wave patterns for forced problems. Combined with the analysis of Floquet-Bloch waves in addition to exponentially localised defect modes, this gives an interesting new observation of chiral patterns in dynamic elastic chains.

The dimensionless chirality parameter, associated with the gyroscopic rate of spin, and the dimensionless pre-tension parameter of the elastic chain together provide the vital means of controlling the waves within the periodic chiral waveguide. It is also shown how Floquet-Bloch waves, which are quasi-periodic by definition, have a geometrical shape that changes, both in the orientation and the eccentricity of the elliptical path of nodal points, as the waves propagate along the chain.

The ideas of the present study are readily applicable to the cases of two- and three-dimensional periodic lattices of different geometries. Of course, in the latter cases, additional technical work is required for the evaluation of chiral dynamic Green's matrices, which inevitably will show the chirality-induced dynamic anisotropy as one of the key features of the dynamic response of such elastic systems.

For reader's convenience, the paper also includes an electronic Supplementary Material video gallery for simulated time-harmonic motions within chiral elastic chains.

References

[1] Moore, J. E., 2010. The birth of topological insulators. Nature **464**, 194-198.

[2] Pendry, J. B., Martin-Cano, D. & Garcia-Vidal, F. J., 2004. Mimicking surface plamons with structured surfaces. Science **305**, 847-848.

[3] Hibbins, A. P., Evans, B. R. & Sambles, J. R., 2005. Experimental verification of designer surface plasmons. Science **308**, 670-672.

[4] Rechtsman, M. C. et al., 2013. Photonic Floquet topological insulators. Nature **496**, 196-200.

[5] Lu, L., Joannopoulos, J. D. & Soljacic, M., 2014. Topological photonics. Nat. Photon. **8**, 821-829.

[6] Wang, Z., Chong, Y., Joannopoulos, J. D. & Soljacic, M., 2009. Observation of unidirectional backscattering-immune topological electromagnetic states. Nature **461**, 772-775.

[7] Pendry J.B., 2000. Negative refraction makes a perfect lens. Phys. Rev. Lett. **85**, 3966-3969.

[8] McPhedran R.C., Movchan A.B. & Movchan N.V., 2009. Platonic crystals: Bloch bands, neutrality and defects. Mech. Mater. **41**, 356-363.

[9] Movchan A.B. & Slepyan L.I. 2007. Band gap Green's functions and localized oscillations, Proc. Royal Soc. A, **463**, 2709-2727.

[10] Carta, G., Jones, I.S., Movchan, N.V. & Movchan, A.B., 2019. Wave Characterisation in a Dynamic Elastic Lattice: Lattice Flux and Circulation. *Phys Mesomech* **22**, 152-163.

[11] Tallarico D., Movchan N.V., Movchan, A.B. & Colquitt D.J., 2017. Tilted resonators in a triangular elastic lattice: Chirality, Bloch waves and negative refraction. Journal of the Mechanics and Physics of Solids, **103**, 236-256.

[12] Chaplain, G.J. , Makwana, M.P. & Craster, R.V. , 2019. Rayleigh-Bloch, topological edge and interface waves for structured elastic plates. Wave Motion, **86**, 162-174 .

[13] Reinbold, J., Frenzel, T., Münchinger, A. & Wegener, M., 2019. The Rise of (Chiral) 3D Mechanical Metamaterials. Materials. **12**(21):3527.

[14] Bahaloo, H. & Li, Y. , 2019. Micropolar modeling of auxetic chiral lattices with tunable internal rotation. J. Appl. Mech. **86**, 041002.

[15] Brun M., Jones I.S. & Movchan A.B., 2012. Vortex-type elastic structured media and dynamic shielding. *Proc. R. Soc. A* **468**, 3027-3046.

[16] Carta, G., Jones, I.S., Movchan, N.V. & Movchan, A.B. 2019. Wave polarization and dynamic degeneracy in a chiral elastic lattice. *Proc. R. Soc. A* **475**, 20190313.

[17] Carta, G. , Jones, I.S. , Movchan, N.V. , Movchan, A.B. & Nieves, M.J. , 2017. Gyro-elastic beams for the vibration reduction of long flexural systems. Proc. Math. Phys. Eng. Sci. **473**, 20170136 .

[18] Carta, G. , Nieves, M.J. , Jones, I.S. , Movchan, N.V. & Movchan, A.B. , 2018. Elastic chiral waveguides with gyro-hinges. Quart. J. Mech. Appl. Math. **71**, 157-185 .

[19] Carta, G. , Nieves, M.J. , Jones, I.S. , Movchan, N.V. & Movchan, A.B. , 2019. Flexural vibration systems with gyroscopic spinners. Phil. Trans. Royal Soc. London **A377**, 20190154.